International Journal of Numerical Methods for Heat and Fluid Flow

Assessment of Turbulence Models for Transonic Oscillating Airfoil

Journal:	*International Journal of Numerical Methods for Heat and Fluid Flow*
Manuscript ID	HFF-04-2016-0142.R3
Manuscript Type:	Research Article
Keywords:	Transonic, Pitching Motion, Turbulence Models, Shock buffeting

Assessment of Turbulence Models for Transonic Oscillating Airfoil

Abstract

Purpose – Computational fluid dynamics (CFD) is applied to study the unsteady transonic flow around a pitch oscillating airfoil, in order to assess the predictive capability of different turbulence models. Accordingly, effects of the amplitude and frequency of the oscillations on aerodynamic coefficients are evaluated.

Design/methodology/approach – Three turbulence models, namely K-ω SST, SAS and DDES, are compared with each other and reported experimental and numerical data. Rigid and sliding movements of the grid are applied to simulate the pitch oscillation and accuracy of the numerical setup is validated based on wind-tunnel data.

Findings – In a certain Mach number, shock-buffet instability occurs when oscillation angle of attack of the model increases up to the buffet onset angle of attack. At this state, airfoil motion interacts with the shock-buffet. DDES shows results that are more accurate in comparison to the results of the SAS and K-ω SST.

Practical implications – The unsteady forces -induced by nonlinear phenomena- may impose large oscillations in aerodynamic coefficients, which may cause strong oscillations of structure and reduced efficient flight zone. Selecting an appropriate turbulent model and reliable estimation of shedding vortices is essential to ensure accurate predictions of aerodynamic forces.

Originality/value – Hybrid RANS-LES turbulence model is applied for simulation of unsteady transonic flow around pitching airfoil and corresponding results are compared with the SAS and RANS simulations. In addition, effects of amplitude and frequency of oscillations on aerodynamic coefficients are evaluated.

Keywords Transonic, Pitching Motion, Turbulence Models, Shock buffeting

Paper type: Research paper

1. Introduction

For certain combinations of the Mach number, airfoil profile and mean angle of attack, large shock oscillations may be occurred in aerodynamic flow over an airfoil, even fixed one. These large shock oscillations are known by buffet. In common airfoils under transonic flow, increasing the pressure value in width of the shock will increase the thickness of the boundary layer at shock foot. At a certain value of pressure, local separation will occur by formation of a bubble at the downstream of the shock. By increasing the free stream Mach number, mentioned separation bubble will firstly behave as a local feature; whereas it would be extended toward the trailing edge. This results in an immediate decrease of the pressure in the trailing edge (pressure divergence). In addition, the shock moves toward leading edge. As the latter goes further upstream into the regions of lower velocities, the shock is weakens and vanishes, the separation point moves downstream to the trailing edge, and the cycle is repeated again. The transonic buffet completely depends on the aerodynamic features, not on the flexible structure. The unsteady forces -induced by the nonlinear phenomena- may impose large oscillations in aerodynamic forces which can make strong oscillations in the structure and reduce the efficient flight zone. In the first researches on the unsteady transonic flow, Tijdeman (1977) studied the interference of the steady and unsteady flows, the oscillating movement of the shock and their effects on the aerodynamic forces. The characteristics of the flow in design point of the supercritical airfoil, where no shock exists, are also investigated in his research. According to the results extracted from the evaluation of the supercritical airfoil NLR 7301 -with the maximum thickness of 16.5 percent of the chord, performing oscillations in pitch around an axis at 40 % of the chord- a considerable interference –correlation- between the steady and unsteady flows are reported. Davis & Malcolm (1979) investigated the distribution of static and dynamic pressure on NACA 64A010 airfoil in transonic and subsonic regimes. In their research, effects of mean angle of attack, Reynolds number, frequency of oscillations and type of the oscillations (Pitching or plunging) were studied. Extending their researches into the evaluation of the supercritical airfoil NLR 7301, they showed that the unsteady aerodynamic coefficients depended on all mentioned parameters. The most important parameters in subsonic flows are Mach number and the oscillation frequency, where in the transonic flows, geometry of the airfoil would be important too. Furthermore, Reynolds number would also be one of the effective parameters in the flows where distinct interference was reported between the shock and the boundary layer. The static and dynamic pressures on the NACA0012 airfoil have been measured by McDevitt & Okuno (1985) with special attention toward the determination of the buffet onset boundary as a function of the flow parameters and of the angle of attack. The authors studied the airfoil in transonic flow with the Mach number of 0.7~0.8 and the Reynolds number of 1×10^6~14×10^6. The sidewall boundary removal has been adopted in the performed wind tunnel tests in order to eliminate the sidewall's effects, such that the resulting streamlines would be more consistent with the free-stream flow and this makes the performed tests to be more

appropriate for CFD validation. Numerical solution of the unsteady transonic flow was firstly performed by Levy Jr. (1978) based on the McDevitt et al. (1976) experimental researches on symmetric circular-arc airfoil. The two-dimensional RANS equations in combination with a primitive algebraic Eddy-viscosity model were solved by finite difference method. Investigations were performed for the Mach numbers of 0.72, 0.754 and 0.783 with the Reynolds number of 11×10^6 to consider both weak and strong shock boundary layer interaction. Regarding the numerical results, the 180°-phase difference between the upper and the lower surfaces, and 20% reduction in shock oscillation frequency are reported in comparison to experimental results. Barakos & Drikakis (2000) adopted some turbulent models for evaluating the experimental researches of McDevitt & Okuno (1985) on the buffet boundaries of NACA0012 airfoil. The experiments were conducted on the Reynolds number of 10×10^6 with the Mach number of 0.7~0.85 by the angle of attack of 0°~5°. Different turbulent models -including algebraic model of Baldwin-Lomax, the one-equation Spalart-Allmaras model, two-equation models of K-ε, and the nonlinear K-ε and K-ω models- were tested. Buffet boundaries were determined by some models as functions of Mach number and the angle of attack. It was reported that the buffet is formed in an angle of attack more than the tested range and the linear K-ε models were unable to simulate all the combinations of the Mach number and the angle of attack. Deck (2005) predicted the transonic buffet on the OAT15A airfoil with the Zonal Detached-Eddy Simulation (ZDES) model. The results were compared with the simulations made by URANS and DES models. That was one of the first researches in which the modeling of the flow features was carried out using DES methods. All three discussed approaches were based on Spalart-Allmaras model. The ZDES model is the only one for predicting the buffet in the experimental angle of attack. In comparison to the URANS models, ZDES is more compatible with the experimental data, especially in the higher frequencies. Capability of nonlinear frequency domain (NLFD) method in predicting details of unsteady transonic flow-fields was investigated by Kharati Koopaee et al. (2010). Results showed that NLFD method could predict reasonable pressure distribution in the time domain except in vicinity of moving shock positions. Some of the results derived by Zonal DES model –presented by Deck (2005)- were compared with the results derived by Delayed DES model for a specific test case by Grossi et al. (2014). Both approaches guarantee a proper switching between RANS and LES during buffet. In the case of that particular ZDES, RANS-mode (using the original SA model) was explicitly imposed in the regions where the grid spacing -in the normal direction to the wall- was smaller than that in the span-wise direction. This ensures that calculation of the shock/boundary interaction must be performed by RANS mode. Maximum levels of pressure fluctuations predicted by the two approaches are similar, despite some differences in the mean shock-wave position and in the amplitude of the shock motion. In the trailing edge region, the fluctuations predicted by the DDES get more intense than those of the ZDES. This behavior can be partially explained by the fact that, in the ZDES, the hybrid RANS–LES formulation was activated only on the upper surface and in the wake. This certainly influences the trailing edge unsteadiness by attenuating or even preventing the alternate vortex shedding seen in the DDES. In recent years,

Szubert et al. (2015) provided a conceptual analysis and a computational model for how the unsteady 'buffeting' phenomenon develops in transonic low incidence flow around a supercritical aerofoil. The amplitude modulation of the buffet and von Kármán modes has been also quantified by POD (Proper Orthogonal Decomposition) analysis. They were shown that, the K-ε-OES model involving an eddy-diffusion coefficient $C_\mu = 0.03$, was able to produce the shock unsteadiness with a frequency close to the experimental one. In this paper, computational fluid dynamics (CFD) is applied to study the unsteady transonic flow around a pitch oscillating airfoil, in order to assess the predictive capability of three different turbulence models, K-ω SST, SAS (Scale Adaptive Simulation) and DDES (Delayed Detached Eddy Simulation), in simulating the nonlinear phenomena such as the shock/boundary layer interaction and shock oscillations. Accordingly, effects of the amplitude and frequency of the oscillations on aerodynamic coefficients are evaluated.

2. Numerical method

2.1. Solver

In this paper, the commercially available finite volume method based CFD package Ansys Fluent 15 with an unsteady compressible and viscous flow solver are employed to simulate the unsteady flow field around the transonic NACA0012 airfoil. The flow simulations are performed using the second-order upwind spatial discretization and a second-order implicit scheme for temporal terms. All the governing equations for the solution variables are solved consecutively and the SIMPLE algorithm is applied as the pressure-velocity coupling algorithm. Diverse factors such numerical scheme, the accuracy and suitability of the turbulence model used, and the choice of run parameters, such as grid and time step can play crucial role in simulate unsteady transonic flow field around considerable airfoil . For the turbulence modelling, several methods including two equational K-ω SST, SAS and DDES with sub-model of K-ω SST are used and their results are compared with the existing experimental and numerical data.

2.2. Turbulence modelling approach

Three different turbulence models are selected and used in this study, based on recent studies on unsteady flow and buffet simulation. The shear-stress transport (SST) model is used in this study, based on Menter (1993). Brief descriptions of SAS and DDES turbulence models are given as follow:

2.2.1. Scale-Adaptive Simulation (SAS):

The Scale-Adaptive Simulation (SAS) is an improved URANS formulation, which allows the resolution of the turbulent spectrum in unstable flow conditions. The SAS concept is based on the introduction of the von Karman length-scale into the turbulence scale equation (Menter & Egorov 2006). The information provided by the von Karman length-scale allows SAS models to be dynamically adjusted for resolved structures in a URANS simulation, which results in a LES-like behaviour in unsteady regions of the flow-field (Menter et al. 2003) (Egorov & Menter 2008). The standard SAS model equations can be written as (Egorov & Menter 2008):

$$\frac{\partial \rho k}{\partial t}+\frac{\partial}{\partial x_j}\left(\rho U_j k\right)=P_k-\rho c_\mu k\,\omega+\frac{\partial}{\partial x_j}\left[\left(\mu+\frac{\mu_t}{\sigma_k}\right)\frac{\partial k}{\partial x_j}\right] \tag{1}$$

$$\frac{\partial \rho \omega}{\partial t}+\frac{\partial}{\partial x_j}\left(\rho U_j \omega\right)=a\frac{\omega}{k}P_k-\rho\beta\omega^2+Q_{SAS}+\frac{\partial}{\partial x_j}\left[\left(\mu+\frac{\mu_t}{\sigma_\omega}\right)\frac{\partial \omega}{\partial x_j}\right]+\left(1-F_1\right)\frac{2\rho}{\sigma_{\omega 2}}\frac{1}{\omega}\frac{\partial k}{\partial x_j}\frac{\partial \omega}{\partial x_j} \tag{2}$$

Compared with SST turbulence model equations, there is only one extra source term, Q_{SAS} , added in ω equation and the rest remains unchanged (Egorov & Menter 2008).

$$Q_{SAS}=\max\left[\rho\zeta_2 kS^2\left(\frac{L}{L_{\nu K}}\right)^2-C.\frac{2\rho k}{\sigma_\Phi}\max\left(\frac{1}{\omega^2}\frac{\partial \omega}{\partial x_j}\frac{\partial \omega}{\partial x_j},\frac{1}{k^2}\frac{\partial k}{\partial x_j}\frac{\partial k}{\partial x_j}\right),0\right] \tag{3}$$

The model parameters in the SAS source term equation are:

$$\zeta_2=3.51\ ,\sigma_\Phi=2/3\ ,C=2$$

Here L is the length scale of the modelled turbulence:

$$L=\frac{\sqrt{k}}{c_\mu^{\frac{1}{4}}.\omega} \tag{4}$$

And the von Karman length scale $L_{\nu K}$ is given by:

$$L_{vK} = k\left|U'(y)\,f\;U''(y)\right| = \frac{\sqrt{2S_{ij}S_{ij}}}{\sqrt{\left(\nabla^2 u\right)^2 + \left(\nabla^2 v\right)^2 + \left(\nabla^2 w\right)^2}} \tag{5}$$

2.2.2. Delayed Detached-Eddy Simulation (DDES):

The Detached-Eddy Simulation, or simply DES, is a hybrid RANS-LES method that was firstly introduced by Spalart et al. (1997). The principle concept of DES is the combination of RANS and LES into a single hybrid turbulence model possessing the best properties of each approach. In its 'natural use' (according to the terminology adopted by Spalart (2005)), attached boundary layers are completely treated in RANS, whereas regions of separated flow are simulated using LES. The switching between the two modes (RANS and LES) is performed by altering the turbulence length scale in the equations: switching between a RANS length scale l_{RANS} -provided by the original model- and a LES length scale l_{LES} -computed upon the local grid size. The effective turbulence length scale l_{DES} in the DES model is then calculated as:

$$l_{DES} = \min\left(l_{RANS}, l_{LES}\right) \tag{6}$$

In the simulation of transonic buffet, the tangential grid spacing should be small enough for a proper resolution of the shock-wave motion region. This can reduce the RANS region to a thin layer around the airfoil when using DES on fine grids. Furthermore, the boundary layer is not permanently separated and becomes considerably thick due to the interaction with the shock wave and to the adverse pressure gradient on the rear part of the airfoil. Therefore, the boundary-layer thickness may get much larger than the RANS region provided by DES. This can result in an erroneous activation of the LES mode inside the boundary layer and potentially leads to modelled-stress depletion (MSD). A general solution to MSD - simple enough to be applied to any eddy-viscosity model- was proposed by Spalart et al. (2006). The improved model detects and 'shields' attached boundary layers by delaying the activation of the LES mode. This is why the model is known by Delayed Detached-Eddy Simulation (DDES). The core of the DDES is the near-wall parameter r_d .

$$r_d \equiv \frac{\nu_t + \nu}{Sk^2 d^2}, S = \sqrt{\frac{\partial U_i}{\partial x_j}\frac{\partial U_i}{\partial x_j}} \tag{7}$$

Where r_d is equal to one in the logarithmic layer and goes to zero as it comes toward the boundary layer edge. The scalar S was chosen as the norm of the whole deformation tensor in order to gain robustness in irrotational regions (Spalart et al. 2006). The introduction of the molecular viscosity in the numerator of r_d corrects the very near-wall behaviour keeping r_d far from zero. The r_d parameter is used to design the delaying function of f_d, which is capable of distinguishing between RANS and LES regions. This function is defined as:

$$f_d = 1 - \tanh[(8r_d)^3] \tag{8}$$

Which is equal to one in LES regions ($r_d \ll 1$) and zero in all other zones. Finally, the DDES length scale is computed by:

$$l_{DDES} \equiv d - f_d \max\left(0, l_{RANS} - l_{LES}\right) \tag{9}$$

On the contrary, the redefinition of the turbulence length scale in DDES makes the method capable of detecting and protecting an attached boundary layer of the LES mode.

2.3. Governing and boundary condition

Figure 1 illustrates the domain dimension, computational grid and applied boundary conditions. The main computational domain is covered by a C-type grid extending 30 chords away (stream-wise x-direction) from trailing edge of the airfoil, 15 chord away from leading edge and approximately 25 chord away (vertical y-direction) from upper and lower surfaces of the airfoil. The test case has been already mentioned by Barakos & Drikakis (2000) and Raveh (2009) with the domain dimension of 7 and 18 chords far from the wall, respectively. In order to insure that the results are grid size independent, different two-dimensional meshes are tasted with the total cell number of 35880, 46020, 65410, 85800 and 105690. Calculations are performed on a flow over NACA0012 airfoil at free stream Mach and Reynolds number of 0.75 and 10×10^6, with the angle of attack of 2° (see Table 1, Set 1). Figure 2 presents the computed pressure coefficient distribution C_p using five different meshes. It can be seen that the total cell number of 85800 is suitable for this study.

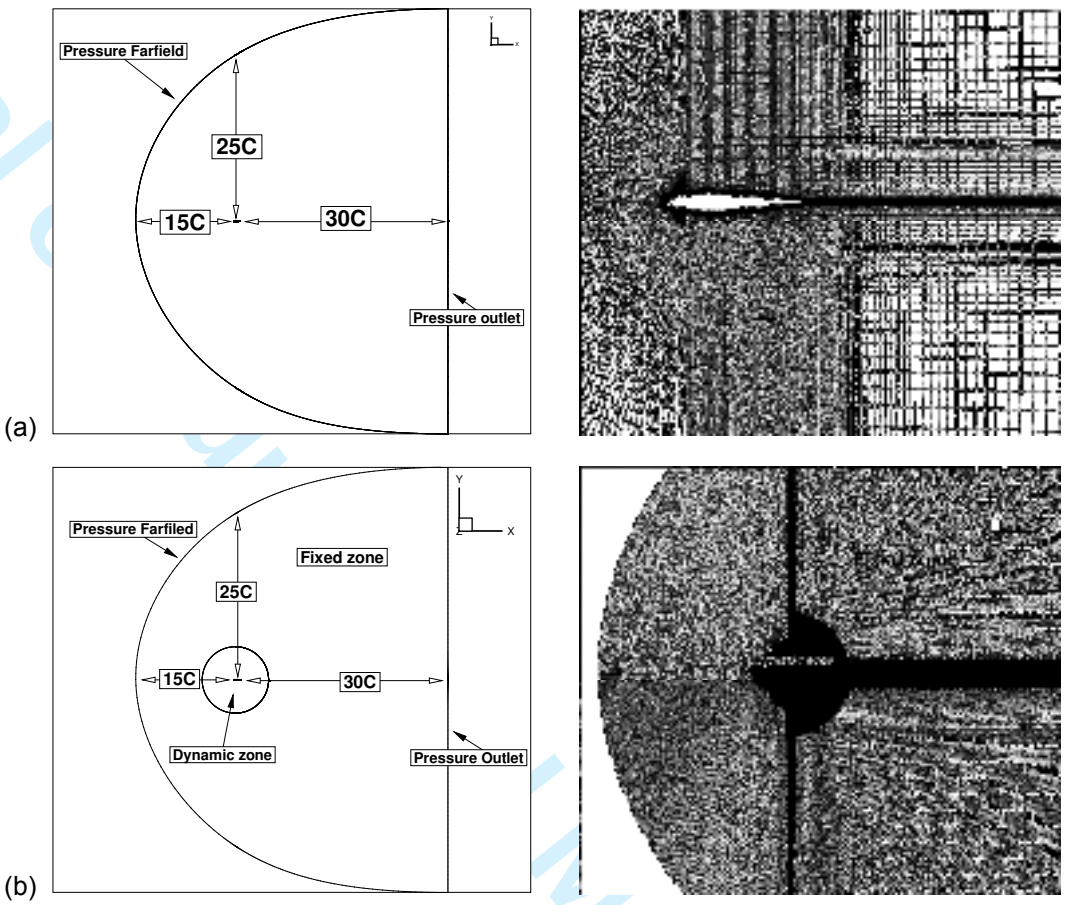

Figure 1 Computational grid and domain; (a) rigid movement for whole domain (b) grid divided into two zones where the first zone is dynamic and the second is fixed

The first cells in contact with solid walls are on average $1\times10^{-5}\,C$ tall in the normal direction to provide y^+ values below or close to one. y^+ is the non-dimensional wall distance for a turbulent boundary layer defined as $y^+ = \frac{\rho u_f y}{\mu}$ (Shojaeefard et al. 2012) and friction velocity u_f is calculated as $u_f = \sqrt{\tau_w / \rho}$. In this equation, ρ is the density and τ_w is the wall shear stress. To find the accuracy of the calculated value for the wall shear stress, the skin friction coefficients C_f of upper and lower surfaces of the NACA0012 airfoil computed with the two-dimensional K-ω SST, are compared to the Iovnovich & Raveh's (2012) RANS simulation results. In both studies, simulations are performed based on McDevitt & Okuno's (1985) wind-tunnel test case with the Mach number of 0.75 and angle of attack of 2° (see Table 1, Set 1). As it is seen in Figure 3, there is a good validity between the computed and Iovnovich & Raveh's (2012) results. So as to pitch oscillation simulation around ¼ airfoil chord, rigid and sliding movement of the grid are applied.

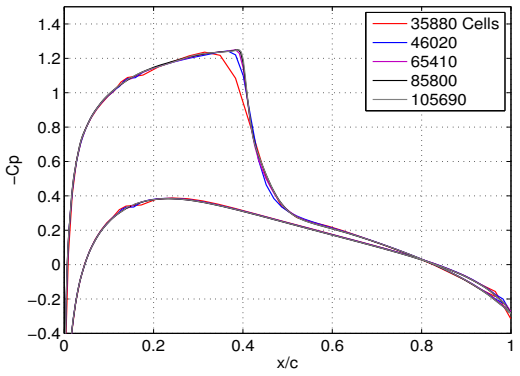

Figure 2 Mesh independency analysis

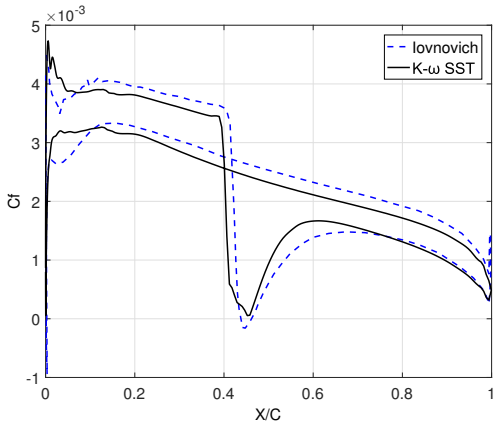

Figure 3 Skin friction coefficient variation of the NACA0012 airfoil, comparison of the K-ω SST and Iovnovich & Raveh's (2012) **results.**

3. Results and discussion

3.1. Two-dimensional fixed airfoil

The wind tunnel tests -performed by McDevitt & Okuno (1985)- and the experimental results presented by Landon (1982), are used to validate the numerical results, which are investigated in this paper by the aid of CFD. Reynolds number of 10×10^6 is selected for the numerical evaluation, based on the research by McDevitt & Okuno (1985). Four main cases of applied information for the mentioned research have been presented in Table (1).

Table 1 Data sets of McDevitt and Okuno's wind-tunnel test

Set	M_N	α_N, deg	M_∞	α, deg
1	0.75	2	0.751	1.99
4	0.8	1	0.793	1.00
5	0.775	2	0.775	2.05
6	0.725	4	0.726	3.91

This information is used for validation of the proposed approach in current paper. The nominal angle of attack and the Mach number, which are used for adjustment of the wind tunnel, have been introduced by subscript of N. The real values of these parameters are shown by α and M_∞. Figure 4 illustrates the pressure coefficient distribution for the upper and lower surfaces of the four mentioned cases, which are calculated with the K-ω SST. It is visible that in all sets except set 4, good agreement is achieved between numerical and experiment results and shock's location is fairly well calculated. The same discrepancy between numerical and experimental results in set 4, was previously reported in other studies ((Iovnovich & Raveh 2012),(Crouch et al. 2009)) using RANS calculations.

Set 1 Set 4 Set 5 Set 6

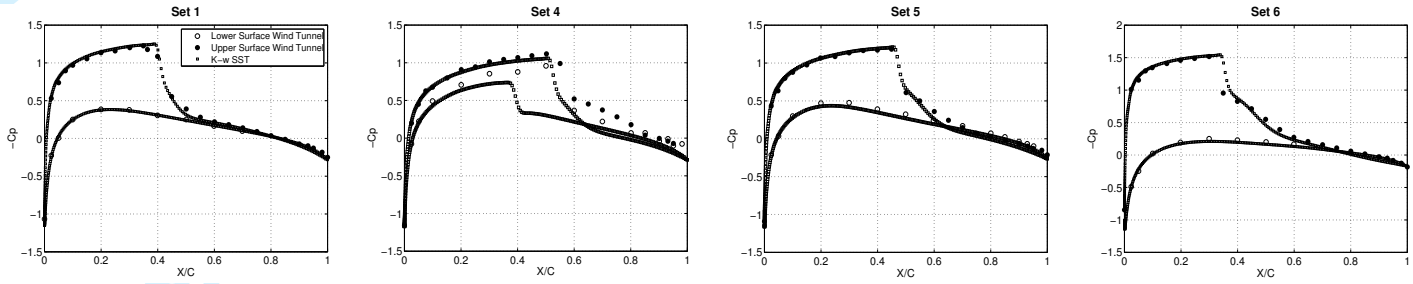

Figure 4 pressure coefficient distribution on NACA0012 airfoil calculated with SST K-ω Turbulence model in comparison to McDevitt & Okuno's (1985) wind-tunnel-tests.

3.2. Two-dimensional oscillating airfoil

In the next step, the pitch motion simulation of the 2D NACA 0012 airfoil around 1/4 chord is performed by two approaches. In the first approach (Mesh 1), the rigid movement is considered for whole domain (Figure 1(a)). The second approach (Mesh 2) according to Figure 1(b) divides the grid into two zones where the first zone is dynamic and the second zone is fixed. The test reduced frequency is defined as:

$$K = \frac{2\pi fc}{U_\infty} \tag{10}$$

Results of the two approaches are compared with the wind tunnel test results presented by Landon (1982). Figure 5 represents the normal force and moment coefficients versus angle of attack in response to prescribed sinusoidal pitch oscillation, with amplitude of 2.51° about a mean angle of attack of 0.016°. Reduced frequency of 0.1628 and Mach number of 0.755 is considered for this case. Simulations are performed using two-dimensional meshes in line with the K-ω SST turbulent model. In order to determine the appropriate time step, a study is carried out with the use of rigid movements of the grid and simulation time steps of 0.005, 0.0005 and 0.000125. As it is seen in Figure 5(a), the time step of 0.0005 or smaller is appropriate for these calculations. The trend of the correlation between experimental and numerical test results is similar to those of other CFD simulations (Raveh 2009). Both of pitch oscillation simulation approaches show agreeable consistency with the experimental results (Figure 5); however, the first approach is selected for the numerical simulation, which is discussed herein.

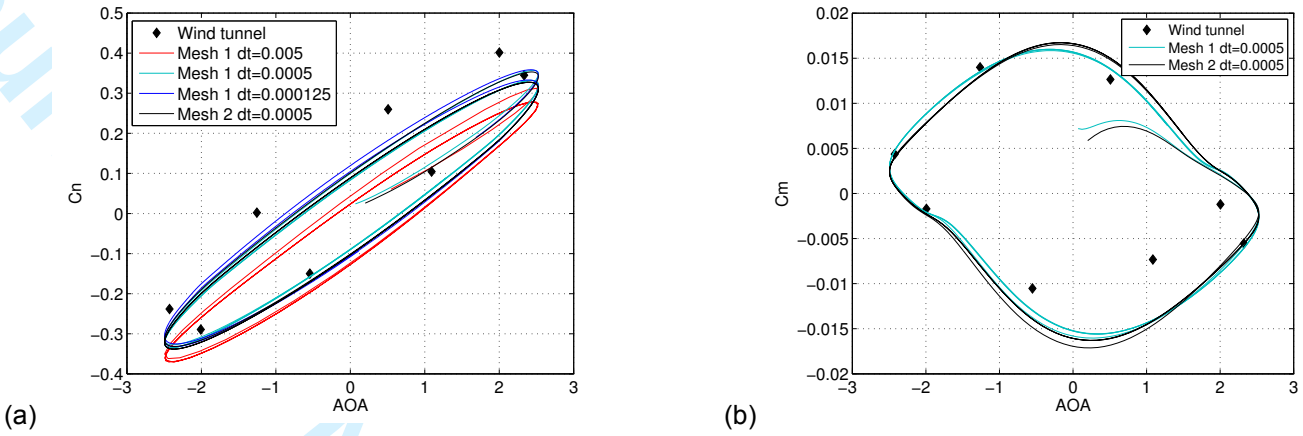

Figure 5 Angle of attack vs (a) normal-force coefficient and (b) moment coefficient about the quarter-chord in response to sinusoidal excitation at $M_\infty = 0.775$, $\alpha = 2.51$ deg, $\alpha_m = 0.016$ deg, $Re = 10^7$, $K = 0.1628$, computed by CFD and recorded at Landon's (1982) wind-tunnel test.

3.3. Two-dimensional oscillating airfoil in buffeting flow-field

Under specific combinations of Mach number and incidence, complex nonlinear phenomena may take place in the flow. Therefore, investigating the numerical solution with two-dimensional K-ω SST model for predicting the nonlinear phenomena -like shock boundary layer interaction and shock oscillations- is of interest. For this purpose, numerical results of Raveh (2009) are selected for validation. Calculations were performed on a flow over pitching NACA0012 airfoil around quarter chord, at free stream Mach and Reynolds number of 0.72 and 10×10^6, with the amplitude of 6° and a mean angle of attack of 0° at various reduced frequencies. Figure 6 presents lift coefficient calculated with k-ω SST model in various reduced frequencies in comparison to Raveh's (2009) results. It can be seen that the oscillating shock appears as a higher-frequency response on top of the oscillation response. By the consecutive for- and back-ward oscillation of the shock, which is followed by separation and re-attachment of the boundary layer, lift coefficient would also consecutively increase and decrease. According to the results presented in Figure 6, in the case of excitations with lower frequencies (Figure 6(a)), the lift coefficient fluctuations on the top of the oscillation response are not predicted as well as those in the case of excitations with higher frequencies -which is close to the calculated buffet frequency- (Figure 6(d)). Fast Fourier Transform of lift coefficient in response to oscillations with reduced frequency of 0.0769, is used to determine the dominant frequency. The buffet reduced frequency is approximately calculated by 0.23. However, the amount of reduced frequency obtained by Raveh (2009) is 0.59. As it is seen in Figure 6, by increasing in excitation frequency up to the buffet frequency (Figure 6(d)): lock-in occurs beyond a certain level of airfoil amplitude, the flow-field response at the buffet frequency is vanished, and the flow system response predominantly assumes the frequency of the airfoil motion. The

airfoil amplitude that will cause lock-in depends on the ratio between the frequency of the airfoil oscillation and the buffet frequency (Raveh 2009).

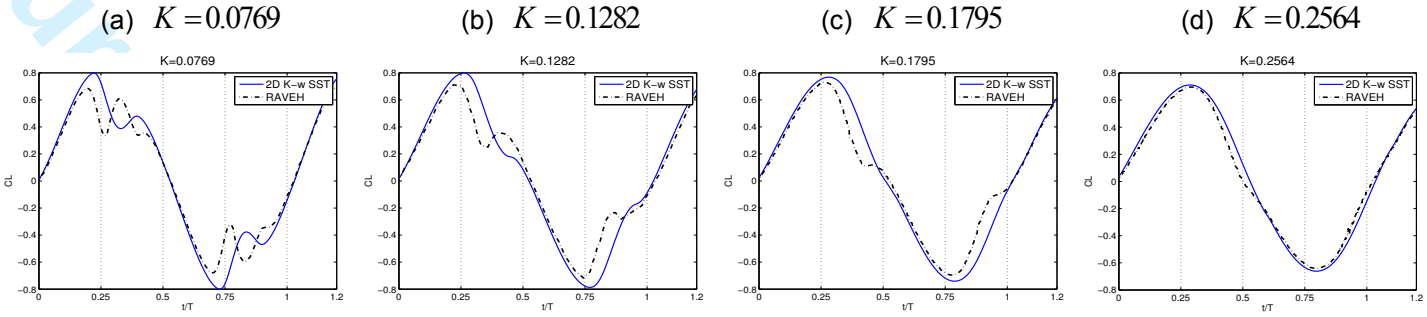

Figure 6 Lift coefficient about the quarter-chord vs reduced time in response to sinusoidal pitching excitations at various frequencies; $M_\infty = 0.72$, $\alpha = 6$ deg, $\alpha_m = 0$ deg, $Re = 10^7$, calculated with K-ω SST turbulent model against Raveh's (2009) results.

3.4. Three-dimensional fixed airfoil in buffeting flow-field

In the previous section, it was observed that at specific value for angle of attack, commonly lower than buffet onset boundary, two-dimensional model of the SST Provides appropriate results while it may be somehow inaccurate at buffet region. Due to the Consecutive for- and back-ward oscillation of the shock, which is followed by separation and re-attachment of the boundary layer, alternative vortex shedding was formed. URANS inherent weakness in simulation of the vortices and their effect on aerodynamic coefficients could be the main reason for this disability. With the aim of proper estimation of flow unsteadiness, DDES and SAS turbulence models were examined. These turbulence models were selected based on recent studies on unsteady flow and buffet simulation. In this way, the first step in the grid generation is to define the airfoil span length L_z. In the present work, the choice of the span length follows the analogy made by Deck (2005). Hence, a span of $L_z = 0.25C$ is adopted in the present simulation. The three-dimensional grid is then obtained by distributing equally spaced copies of the planar grid presented in Figure 1(a) in the span-wise direction. To obtain $\Delta k \approx \Delta i$ over the rear part of the airfoil and in the near of the wake, 40 grid cells have been generated in the span-wise direction, resulting in a three-dimensional grid with approximately 3.2-million cells. Investigation on buffeting flow-field over fixed NACA0012 airfoil in free stream Mach number of 0.72 and angle of attack of 6° is performed with DDES approach. As expected, the DDES simulation predicts the self-sustained large-scale shock wave motion at the experimental angle of attack of 6° (McDevitt & Okuno 1985). The time histories of the lift coefficient and moment coefficient about ¼ chord are presented in Figure 7(a). The oscillations are due to the buffet. Shock wave oscillates and interacts with the boundary layer, consecutive separation and reattachment of the boundary layer occurs and results to the oscillation of the aerodynamic coefficients. The mean lift coefficient equals 0.44, and the moment coefficient, which is computed about the ¼ chord, more often is positive throughout the cycle because shock is oscillated in downstream of the ¼-chord point. As it can

be noted, the amplitude of the fluctuations also varies from one cycle to the other. Fast Fourier Transform of lift coefficient is presented in Figure 7(b). Buffet reduced frequency is approximately calculated by 0.5484 against buffet reduced frequency of 0.55 presented by McDevitt & Okuno (1985), which have less than 1% error.

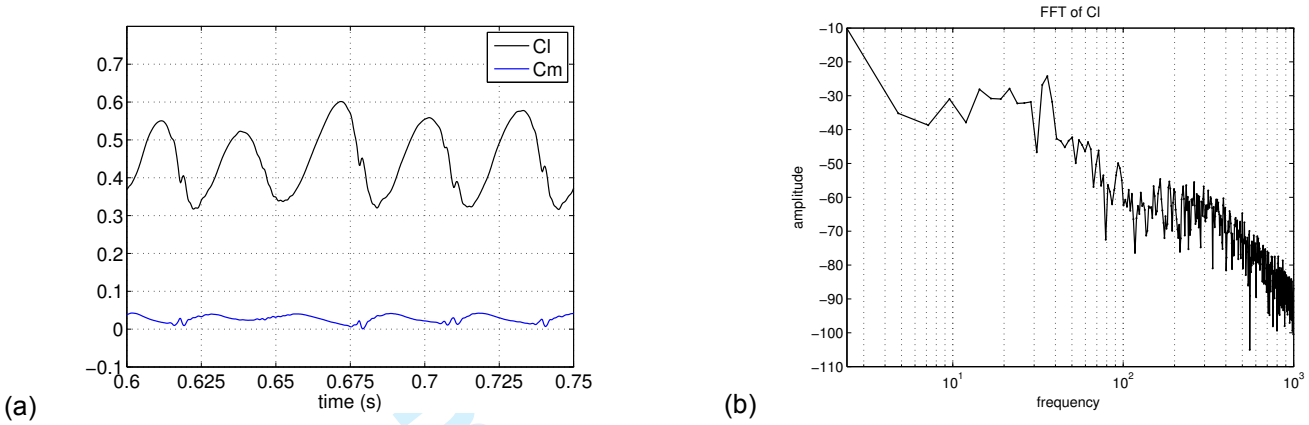

(a) (b)

Figure 7 (a) Lift and moment coefficient in a buffeting flow vs time (s) (b) FFT of lift coefficient; $M_\infty = 0.72$, $\alpha = 6$ deg, $Re = 10^7$

3.5. Three-dimensional oscillating airfoil in buffeting flow-field

Figure 8 presented variation of lift coefficient versus reduced time, and angle of attack in response to reduced excitation frequency of 0.0769 and amplitude of 6°, calculated with DDES and SAS model against numerical results by Raveh (2009). As it is shown in Figure 8(a), the DDES turbulent model expresses more appropriate results; however, the SAS models (like SST simulation) are not efficient enough in evaluating the characteristics of the nonlinear flow (Grossi et al. 2014). It can be seen that the lift coefficient increases with increasing angle of attack. With further increase in angle of attack, shock power is increased and interaction between strong shock and boundary layer leads to separation of the boundary layer in the shock foot; accordingly, the shock moves toward the leading edge. As the shock and the separated region move upstream, the local velocities -ahead of the shock- are increased and the shock becomes stronger. As the latter goes further upstream into regions of lower velocities, it weakens and vanishes, and the separation point moves downstream to the trailing edge and the cycle is repeated again. This consecutive for- and back-ward oscillation of the shock and separation point, which is followed by separation and re-attachment of the boundary layer leads to consecutive increase and decrease in lift coefficient. In the following, by decreasing the angle of attack, shock power is decreased, boundary layer becomes steady, and lift coefficient is also decreased. Frequency analysis of lift coefficients are performed and indicate the buffet reduced frequency of 0.68 for the DDES and 0.23 for SAS (the Raveh's (2009) URANS calculation resulted 0.59). It can be noted that the buffet reduced frequency, which is calculated by the DDES, is increased about 0.13 from fixed airfoil to oscillating one (figure 7(b)). Different calculation of buffet frequency brings about performance difference of turbulence models in calculation of lift coefficient at angle of attacks inside the buffet boundaries. It can be

seen that in Figure 8(a), the lift coefficient signal calculated with the DDES model has more noticeable third pick in comparison to the Raveh's (2009) calculation, which is caused by the higher estimation of the buffet frequency. In addition, Maximum and minimum peaks of lift fluctuations are appeared sooner in DDES. The amplitude of these fluctuations is greater as well. This matter is clearly visible in figure (8b) about angle of attack of -4°.

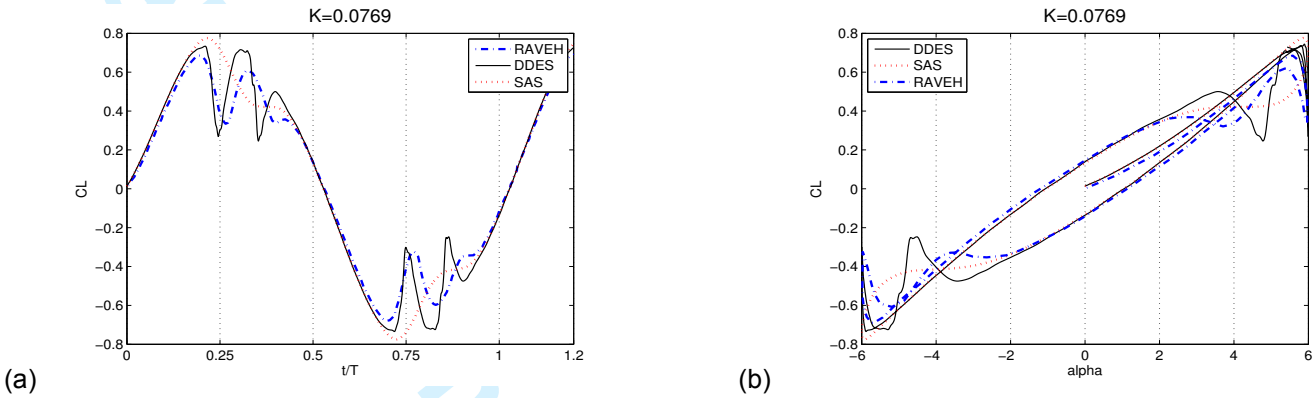

Figure 8 Lift coefficient vs (a) reduced time (b) angle of attack in response to sinusoidal excitation at;

$$M_\infty = 0.72,\ \alpha = 6 \text{ deg},\ \alpha_m = 0 \text{ deg},\ Re = 10^7,\ K = 0.0769$$

3.6. Physics of flow-field and effects of frequency and amplitude of oscillations

For better understanding of physics of transonic flow over an oscillating airfoil, Figure 9 represents 12 phases of flow condition in one excitation cycle. Figure 10 illustrates x velocity and streamlines over airfoil and Figure 11 presents velocity profile in x/C=0.41, which are related to those 12 phases in response to the excitation with reduced frequency of 0.0769. These 12 phases are selected to cover all changes (increases and decreases) in lift coefficient. As it is seen in Figure 10, in phase 01, shock wave was not strong enough to separate the boundary layer; however, increase in the thickness of the boundary layer is visible (Figure 11(a)). By increasing the angle of attack and shock power, in phase 2 (Figure 10), separation of the boundary layer is observed from shock foot toward the trailing edge. In addition, shock moves toward the leading edge. As it is seen in Figure 11(b), the x-component of velocity has a negative value near the wall. As the shock goes further upstream into regions of lower velocities, it weakens and vanishes, and the separation point moves downstream to the trailing edge (Figure 10 (Phase 03)). Meanwhile, the boundary layer becomes reattached (Figure 11(c)). The maximum downstream location is achieved for shock and separation bubble is then formed at the foot shock. In phase 04, separation is formed from shock foot until trailing edge by the travel of the shock toward the leading edge (Figure 10 (Phase 04) and Figure 11(d)). In the following, with decrease in angle of attack, shock becomes weaker and in phase 5, only a small separation bubble can be seen at the foot shock (Figure 10 (Phase 05) and Figure 11(e)). In this angle of attack, in upstroke motion, boundary layer has been attached. It's shown that, there is an asymmetry

between phenomenon in pitch up and pitch down motion, in terms of the angle of attack; in other words, shock disappearance occur during pitch down motion at lower angles of attack, in comparison to the occurrence of shock appearance during pitch up. With farther decrease in angle of attack, shock power gradually losses and at the angles of attack about 0° (phase 06), shock is disappeared and boundary layer is attached (Figure 10 (Phase 06) and Figure 11(f)). In the following, the same trend can be seen on the lower surface.

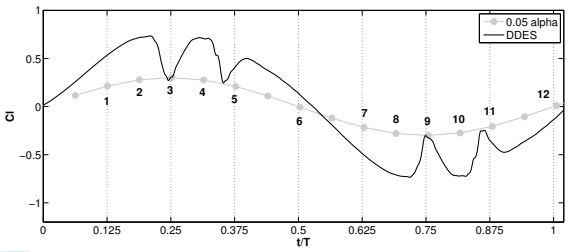

Figure 9 Selected 12 phases of flow condition $M_\infty = 0.72$, $\alpha = 6$ deg, $\alpha_m = 0$ deg, $Re = 10^7$, $K = 0.0769$

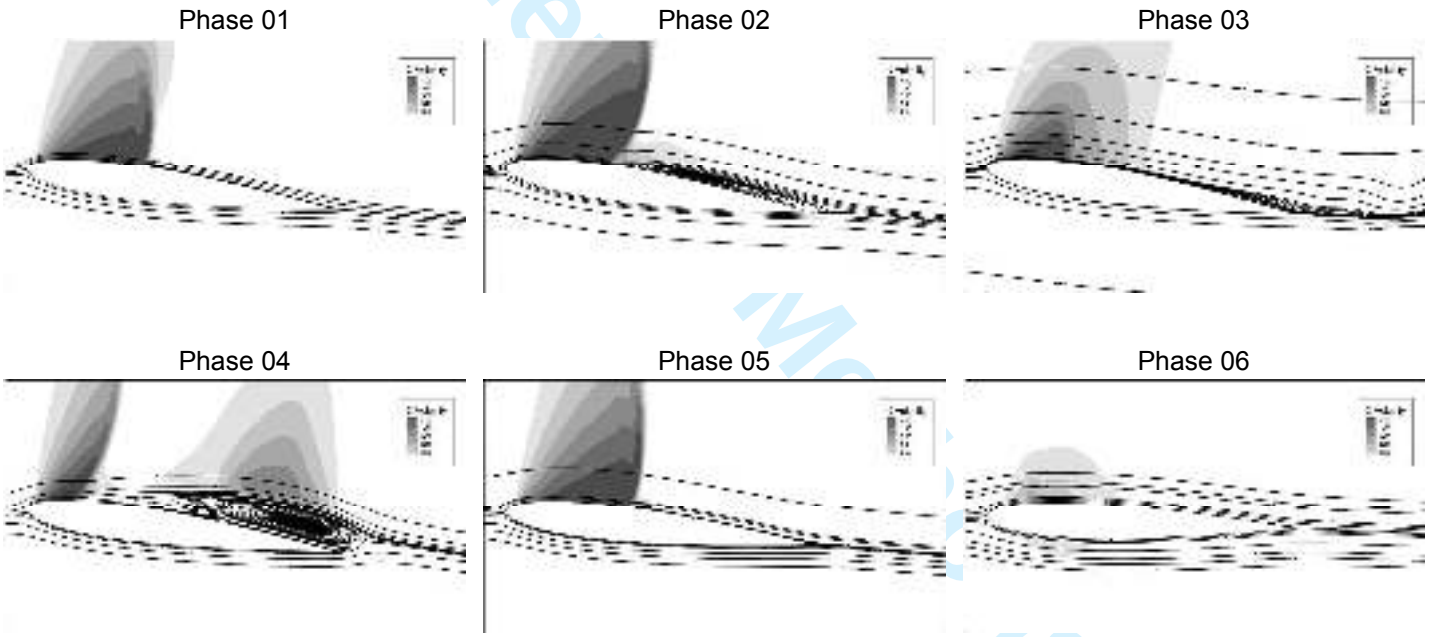

Figure 10 Flow streamlines and x velocity maps during half oscillation cycle;

$M_\infty = 0.72$, $\alpha = 6$ deg, $\alpha_m = 0$ deg, $Re = 10^7$, $K = 0.0769$

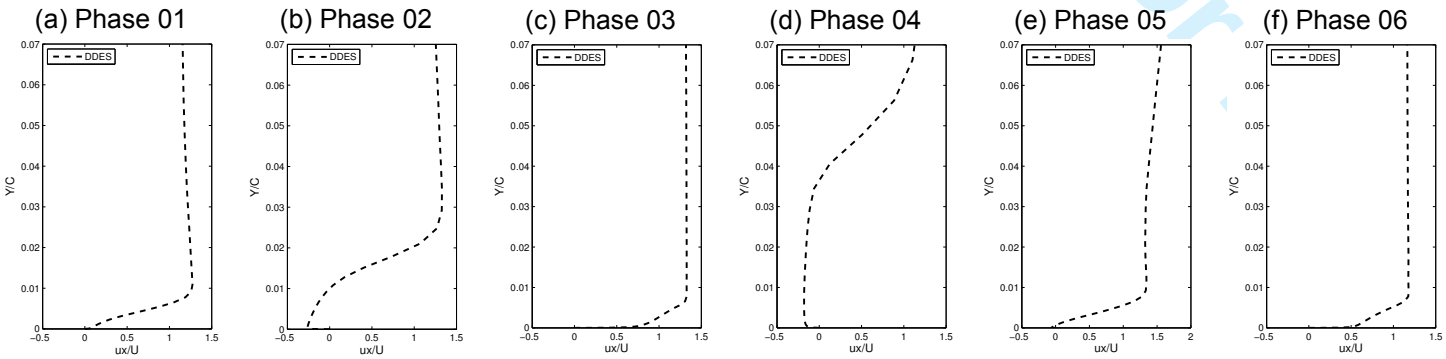

Figure 11 x velocity profile at x/C=0.41 on upper surface; $M_\infty = 0.72$, $\alpha = 6$ deg, $\alpha_m = 0$ deg, $Re = 10^7$, $K = 0.0769$

In the next step, effects of reduced frequencies and amplitude of oscillations are investigated on the aerodynamic behavior of airfoil. In this way, studies are performed with DDES turbulence model in Mach and Reynolds number of 0.72 and $10x10^6$. Sinusoidal oscillations are concerned with various reduced frequencies, mean angle of attack equal to 0°, and amplitudes of oscillation of 6° and 8°. Figure 12(a~e) and Figure 13(a~e) illustrate variation of the lift coefficient with reduced time and angle of attack. In lower reduced frequencies, which are far from buffet frequency, effects of unsteadiness on aerodynamic coefficients are followed with higher-frequency responses on top of the oscillation response (Figure 12(a and b)). As it is seen in Figure (12c~e), by increasing in excitation frequency up to the buffet frequency, the phase difference between shock and airfoil motion will lead in reduction of unsteadiness's effect on aerodynamic coefficients. Therefore, fluctuations of lift coefficient decrease. Moreover, influence of shock oscillations on lift coefficient appears in lower angle of attacks (Figure 13). By increasing in the amplitude of oscillation -from 6° to 8°- more variations are reported in aerodynamic coefficients. This is due to the increase in the time duration that the airfoil remains at the angle of attacks inside the buffet boundaries. This means that, the shock has more time to oscillate back and forth (Figure 12). Frequency analysis of calculated lift coefficient -in response to the excitations with reduced frequencies of 0.05 and 0.0769 (Figure 14(a)) and amplitude of 6° and 8° (Figure 14(b)) - is conducted. The first peak introduce the excitation frequency. The results illustrate that: By increasing the excitation frequencies and amplitude of oscillations, buffet reduced frequency will not change significantly and will be reported by the same value of 0.68.

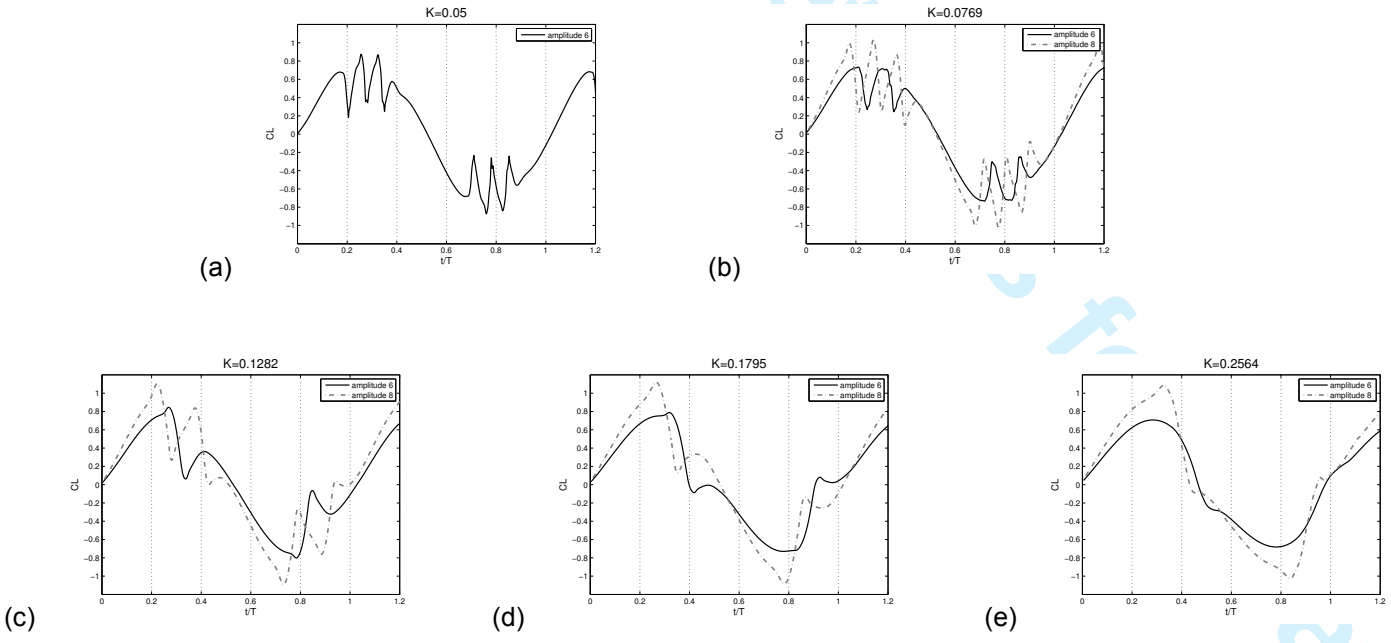

Figure 12 Lift coefficient vs reduced time in response to sinusoidal excitation at various amplitude and frequencies; $M_\infty = 0.72$, $\alpha = 6$ and 8 deg, $\alpha_m = 0$ deg, $Re = 10^7$

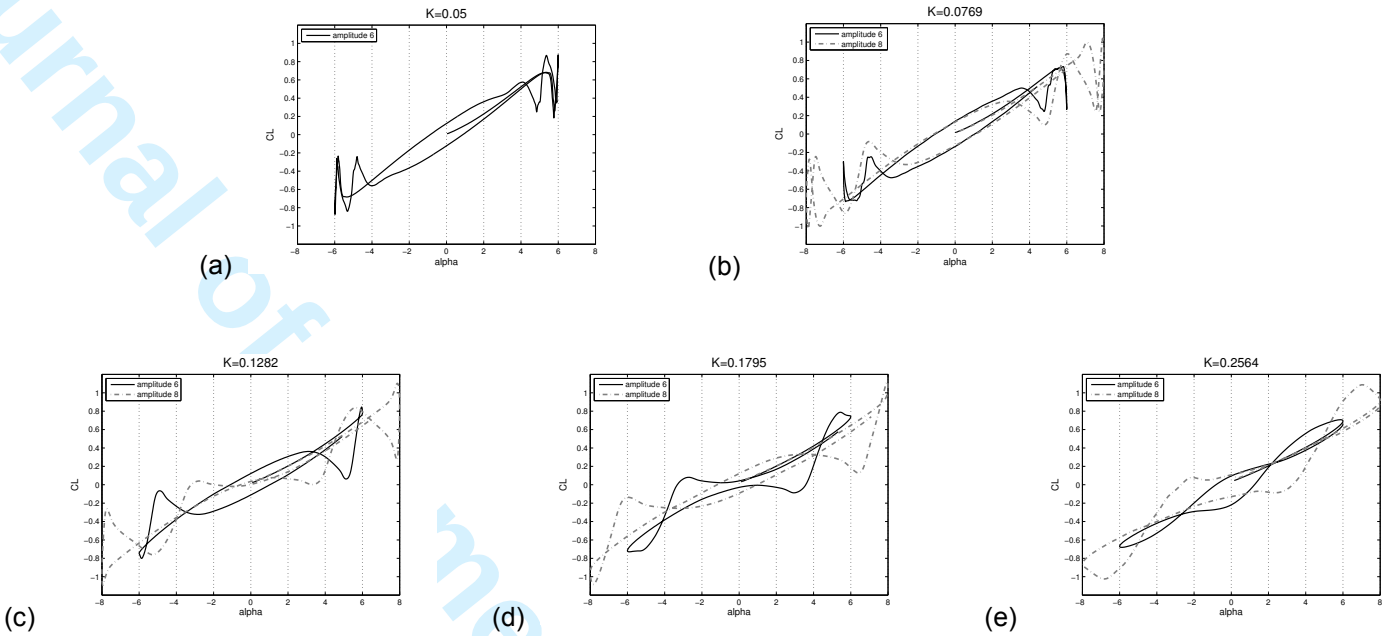

Figure 13 Lift coefficient vs angle of attack in response to sinusoidal excitation at various amplitude and frequencies; $M_\infty = 0.72$, $\alpha = 6$ and 8 deg, $\alpha_m = 0$ deg, $Re = 10^7$

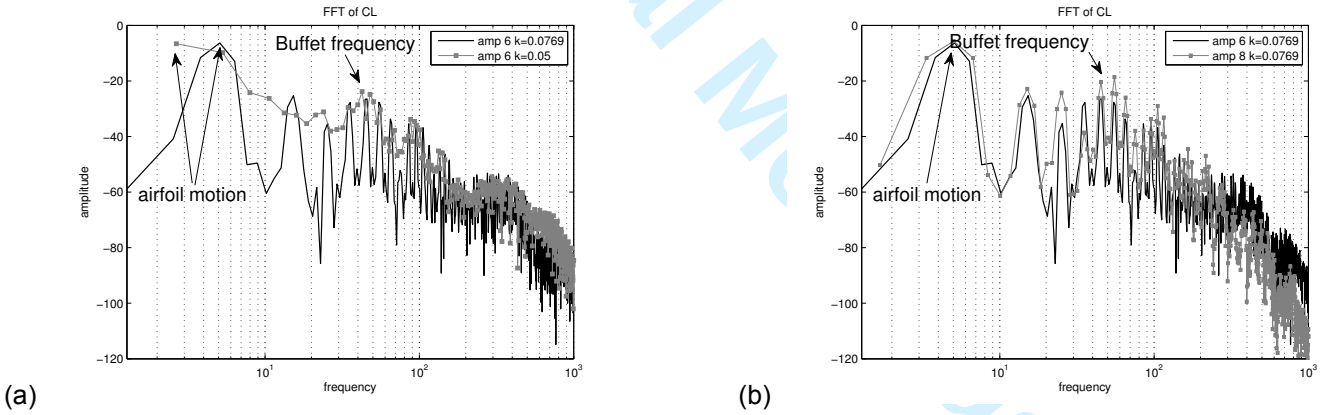

Figure 14 FFT of lift coefficient in response to sinusoidal excitation at; $M_\infty = 0.72$, $\alpha_m = 0$ deg, $Re = 10^7$ a) $\alpha = 6$ deg $K = 0.0769$ and 0.05 b) $\alpha = 6$ and 8 deg, $K = 0.0769$

3.7. Comparison between turbulence models

In previous sections, it was observed that in the angles of attack -lower than buffet boundary- two-dimensional model of the SST provides appropriate results and its disabilities are shown at buffet region. The three-dimensional SAS turbulence model either. It was demonstrated that the DDES model provides acceptable results for modeling both shock oscillations and vortex shedding in buffet region. For better understanding, Figure 15 presents the pressure coefficient distribution

over the airfoil in phases 01 and 02, specified in Figure 9. In the angles of attack, specifically lower than the buffet onset (phase 01), it can be seen that pressure coefficient distribution and shock location are calculated almost as the same way by all three models (Figure 15(a)). In phase 02, SST and SAS turbulence models calculate the shock location and pressure coefficient distribution almost equally (Figure 15(b)). However, as it is seen in Figure (15(b)), DDES model determines shock location closer to the leading edge. In addition, the pressure coefficient divergence is observed in simulation by DDES approach. Figure 16 presents Eddy viscosity ratio near the airfoil in phases 01, 02 and 03, where Figure 17 presents the velocity profile and Eddy viscosity ratio in x/C=0.41. As it is expected, in phase 01, all three turbulence models act in a same way. However, Figure 16 shows that the SST model is more dissipative than the others. In phase 02, the SST and SAS models seem to delay the production of eddy viscosity, in comparison to the DDES. This difference may explain why the SST and SAS have predicted the shock-wave location further downstream (Figure 16 (Phase 02)). This delay can be illustrated in better way in Figure 17. Where the flow reversal in x/C=0.41 is calculated with DDES approach and is more intensified in comparison to the SST and SAS results. This delay in the production of Eddy viscosity terms -in the sinusoidal oscillation cycle- is continued and intensified, and is resulted to lack of ability of SST and SAS model to predict the separation and reattachment of boundary layer (unlike the DDES model). It is remarkable that mentioned parameters affect on aerodynamic coefficients in the buffet region. Figure 18 is presented to show the pressure coefficient signals of three points of airfoil's upper surface in response to the sinusoidal oscillation in reduced frequency of 0.0769 and oscillation amplitude of 6°. In early part of the airfoil, boundary layer is often attached and pressure coefficient varies harmonically with airfoil motion. By moving toward downstream, in x/C=2/15, separation and reattachment of boundary layer around t=0.05 are predicted by DDES approach, in contrary to the SST and SAS models due to shock oscillation. In x/C=5/15, it can be seen that the DDES approach predicts the separation earlier and its duration time is greater than the other two methods. With further move toward the downstream, it is observed that the boundary layer is often separated and variation of pressure coefficient is not harmonically any more.

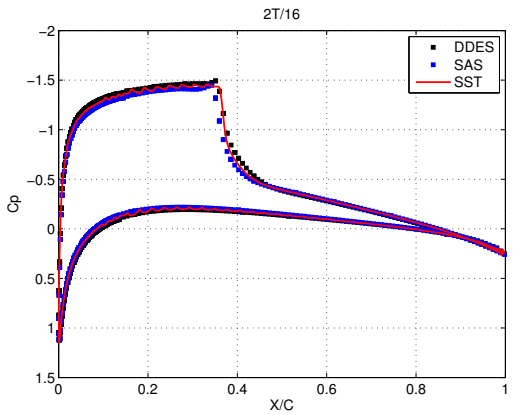

(a) Phase 01

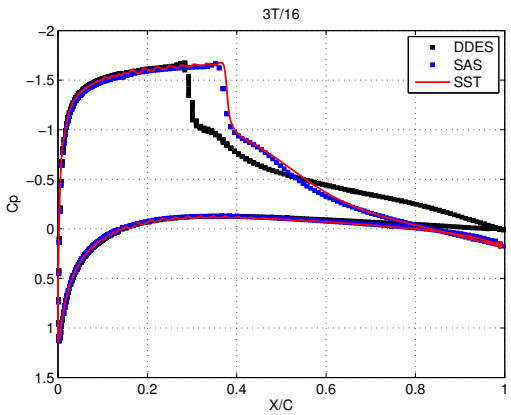

(b) Phase 02

Figure 15 Pressure coefficient distribution in (a) $\frac{2T}{16}$ (b) $\frac{3T}{16}$ for various turbulence models

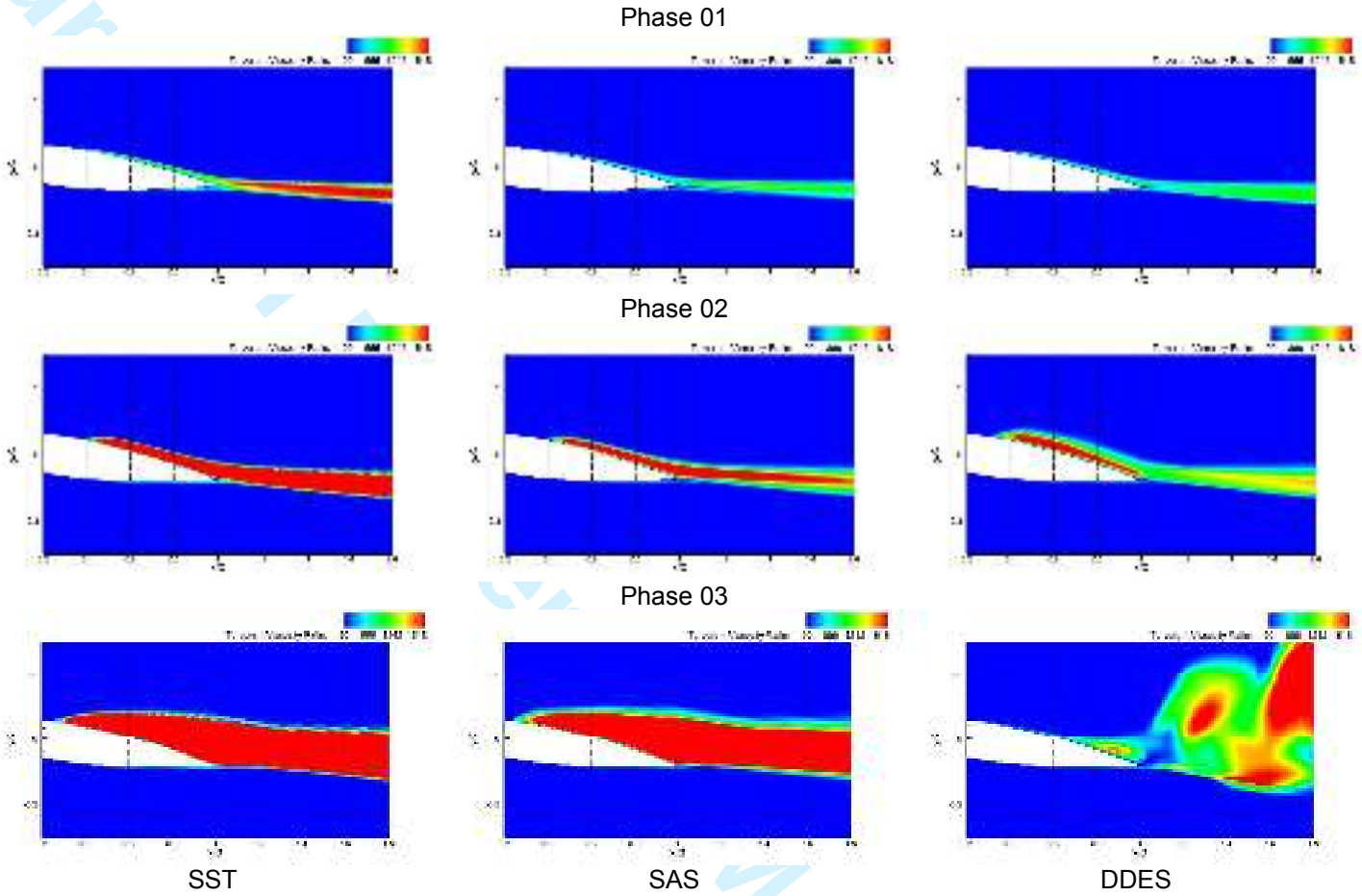

Figure 16 Viscosity ratio distribution for various turbulence models

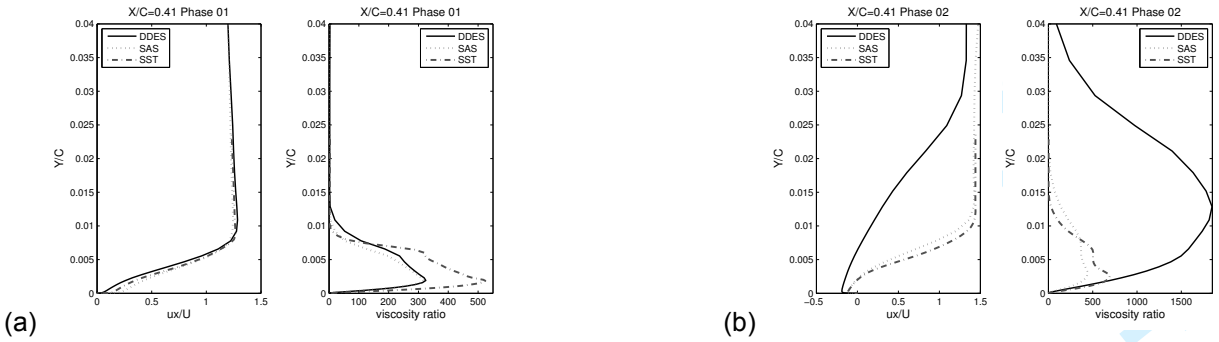

Figure 17 x velocity and viscosity profile at x/C=0.41 (a) Phase 01 (b) Phase 02

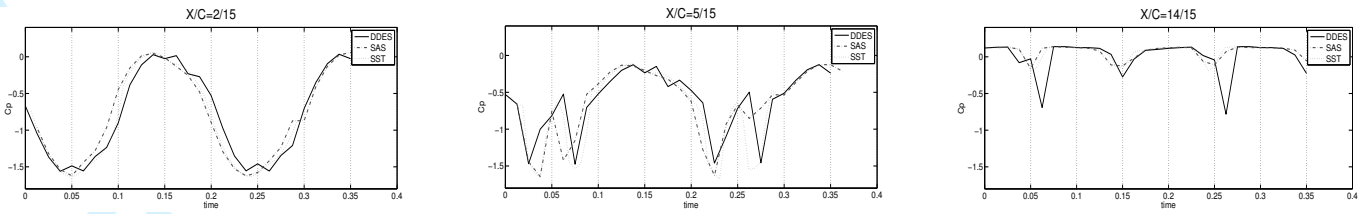

Figure 18 Pressure coefficient distribution vs time (s) on upper surface at various positions

4. Conclusion

In this research study, numerical solution of transonic flow around pitching NACA0012 airfoil was investigated. Accordingly, effects of the amplitude and frequency of oscillations on aerodynamic coefficients were evaluated and the efficiency of the turbulent models, K-ω SST, SAS and DDES, in simulation of the nonlinear phenomena –i.e. the interaction between shock and boundary layer and the shock oscillations- were studied and led to following conclusions:

- At specific value of angle of attack, commonly lower than buffet boundary, two-dimensional model of the SST provided appropriate results while it might be somehow inaccurate at buffet region.

- According to the results inside the buffet boundaries, the DDES turbulent model expressed results that are more appropriate; however, the SAS models (like SST simulation) were not efficient enough in evaluating the characteristics of the nonlinear flow.

- In buffet regions, it seems that SST and SAS models delayed the production of eddy viscosity, in comparison to the DDES. This delay in the production of Eddy viscosity terms -in the sinusoidal oscillation cycle- is continued and intensified, and caused the lack of ability of SST and SAS model to predict the separation and reattachment of boundary layer (unlike the DDES model). It is remarkable that mentioned parameters affected the aerodynamic coefficients in the buffet region.

- With increasing in excitation frequency up to the buffet frequency, lock-in occurred. The phase difference between shock and airfoil motion led in reduction of unsteadiness's effect on aerodynamic coefficients.

- By increasing in the amplitude of oscillation -from 6° to 8°- more variations were obtained in aerodynamic coefficients. The results illustrated that by increasing the excitation frequencies and amplitude of oscillations in

studied domain; buffet reduced frequency would not change significantly. However, 0.13 increase in buffet frequency was reported in comparison to the fixed airfoil.

- In response to the sinusoidal excitations up to the buffet onset, in early part of the airfoil, boundary layer was often attached and pressure coefficient varied harmonically with airfoil motion. With further move toward the downstream, it was observed that the boundary layer was often separated and variation of pressure coefficient was not harmonically any more.

Appendix A: Effect of simulation time step on buffet responses

To study the effect of the simulation time step on buffet responses over oscillating airfoil, simulations were run using computational time steps ranging from 0.000125 to 0.001. Calculations were performed on the flow over pitching NACA0012 airfoil around quarter chord, at free stream with Mach and Reynolds numbers of 0.72 and $10x10^6$ with amplitude of 6° and a mean angle of attack 0° at reduced frequency of 0.0769. Figure 19 presents the time histories of lift coefficient. Figure 19 shows that the unsteady response converges with decreasing time step and that a computational time step of 0.00025 or less, is adequate enough for these types of analyses.

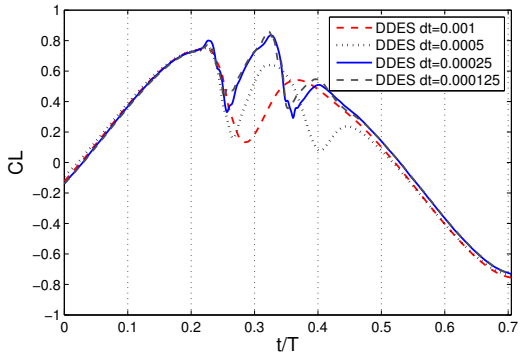

Figure 19 Unsteady response to sinusoidal excitation at; $M_\infty = 0.72$, $\alpha = 6$ deg, $\alpha_m = 0$ deg, $Re = 10^7$, $K = 0.0769$

References

Barakos, G. & Drikakis, D., 2000. Numerical simulation of transonic buffet flows using various turbulence closures. *International Journal of Heat and Fluid Flow*, 21(5), pp.620–626.

Crouch, J.D. et al., 2009. Origin of transonic buffet on aerofoils. *Journal of Fluid Mechanics*, 628, pp.357–369. Available at: http://www.journals.cambridge.org/abstract_S0022112009006673.

Davis, S.S. & Malcolm, G.N., 1979. Experiments in unsteady transonic flow. In *ASME/ASCE/AHS 20th Structures, Structural Dynamics and Materials Conference*.

Deck, S., 2005. Numerical Simulation of Transonic Buffet over a Supercritical Airfoil. *AIAA Journal*, 43(7), pp.1556–1566. Available at: http://arc.aiaa.org/doi/abs/10.2514/1.9885.

Egorov, Y. & Menter, F., 2008. Development and application of SST-SAS turbulence model in the DESIDER project. In *Advances in Hybrid RANS-LES Modelling*. pp. 261–270. Available at: http://link.springer.com/10.1007/978-3-540-77815-8_27.

Grossi, F., Braza, M. & Hoarau, Y., 2014. Prediction of Transonic Buffet by Delayed Detached-Eddy Simulation. *AIAA Journal*, 52(10), pp.2300–2312. Available at: http://arc.aiaa.org/doi/abs/10.2514/1.J052873.

Iovnovich, M. & Raveh, D.E., 2012. Reynolds-Averaged Navier-Stokes Study of the Shock-Buffet Instability Mechanism. *AIAA Journal*, 50(4), pp.880–890.

Kharati Koopaee, M., Alishahi, M.M. & Emdad, H., 2010. Analysis of pressure field in time domain using nonlinear reduced frequency approach in unsteady transonic flows. *International Journal of Numerical Methods for Heat & Fluid Flow*, 20(6), pp.655–669. Available at: http://www.emeraldinsight.com/doi/full/10.1108/09615531011056818.

Landon, R.H., 1982. NACA0012 Oscillatory and Transient Pitching in Compendium of Unsteady Aerodynamics Measurements. *AGARD TR R-701*.

Levy Jr., L.L., 1978. Experimental and Computational Steady and Unsteady Transonic Flows about a Thick Airfoil. *AIAA Journal*, 16(6), pp.564–572. Available at: http://arc.aiaa.org/doi/abs/10.2514/3.60935.

McDevitt, J.B., Levy Jr., L.L. & Deiwert, G.S., 1976. Transonic Flow about a Thick Circular-Arc Airfoil. *AIAA Journal*, 14(5), pp.606–613. Available at: http://arc.aiaa.org/doi/abs/10.2514/3.61402.

McDevitt, J.B. & Okuno, A.F., 1985. *Static and Dynamic Pressure Measurements on a NACA 0012 Airfoil in the Ames High Reynolds Number Facility*,

Menter, F.R., 1993. Zonal Two Equation k-w, Turbulence Models for Aerodynamic Flows. In *AIAA paper*. p. 2906. Available at: http://arc.aiaa.org/doi/10.2514/6.1993-2906.

Menter, F.R. & Egorov, Y., 2006. Revisiting the turbulent scale equation. In *IUTAM Symposium on One Hundred Years of Boundary Layer Research*. pp. 279–290. Available at: link.springer.com/10.1007/978-1-4020-4150-1_27.

Menter, F.R., Kuntz, M. & Bender, R., 2003. A scale-adaptive simulation model for turbulent flow predictions. In *41st Aerospace Sciences Meeting and Exhibit*. pp. 1–11. Available at: http://arc.aiaa.org/doi/10.2514/6.2003-767.

Raveh, D.E., 2009. Numerical Study of an Oscillating Airfoil in Transonic Buffeting Flows. *AIAA Journal*, 47(3), pp.505–515. Available at: http://arc.aiaa.org/doi/abs/10.2514/1.35237.

Shojaeefard, M.H. et al., 2012. Numerical investigation on effects of induced jet on boundary layer and turbulent models around airfoils. *Heat and Mass Transfer*, 48(6), pp.1057–1070. Available at: http://link.springer.com/10.1007/s00231-011-0961-y.

Spalart, P., 2005. The uses of DES: natural, extended, and improper. *Proceedings of Invited presentation at the DESider Hybrid RANS-LES Symposium*.

Spalart, P.R. et al., 2006. A New Version of Detached-eddy Simulation, Resistant to Ambiguous Grid Densities. *Theoretical and Computational Fluid Dynamics*, 20(3), pp.181–195. Available at: http://link.springer.com/10.1007/s00162-006-0015-0.

Spalart, P.R. et al., 1997. Comments on the feasibility of LES for wings and on a hybrid RANS/LES approach. *Advances in DNS/LES*, 1(JANUARY), pp.137–147.

Szubert, D. et al., 2015. Shock-vortex shear-layer interaction in the transonic flow around a supercritical airfoil at high Reynolds number in buffet conditions. *Journal of Fluids and Structures*, 55, pp.276–302.

Tijdeman, H., 1977. Investigation of the transonic flow around oscillating airfoils. *National Aerospace Lab. Amsterdam, Netherlands*, TR-77-090U.

Nomenclature

Symbols

C airfoil chord

C_L lift coefficient

C_m momentum coefficient

C_p pressure coefficient

M_∞ freestream Mach number

U_∞ freestream velocity magnitude

f frequency, Hz

K reduced frequency $\frac{2\pi fc}{U_\infty}$

α angle of attack

α_m mean angle of attack

l turbulence length scale

Δ grid spacing

y^+ nondimensional wall distance

L_z span length

ν kinematic viscosity

ν_t eddy viscosity

T airfoil oscillation cycle period

k turbulence kinetic energy

ω turbulence eddy frequency

S_{ij} strain rate tensor

M_N numerical Mach number

α_N numerical angle of attack

C_μ eddy-diffusion coefficient

Definitions, Acronyms and Abbreviations

Large Eddy Simulation (LES)

Detached Eddy Simulation (DES)

Delayed Detached Eddy Simulation (DDES)

Zonal Detached Eddy Simulation (ZDES)

Reynolds Average Navier Stocks (RANS)

Scale Adaptive Simulation (SAS)

Modelled Stress Depletion (MSD)

Shear Stress Transport (SST)

Comment:

The manuscript presents some results on a NACA0012 aerofoil with sinusoidal pitch oscillation at transonic regime. The manuscript is the revised version of a previous submission, was reviewed by this referee. I am satisfied by the response, has been provided by the authors to address my comments. However, the response on my first comment about *"How the friction velocity (or wall shear stress) is calculated"? And "How accurate is the calculated value?"* (Including Figure 1 on the response) should be accommodated into the manuscript.

Response:

Dear Referee

First, thank you for your useful comments and suggestions that allowed us to greatly improve the quality of the manuscript during these revisions. We are very glad that our response could answer your questions and satisfy your expectations.

According to the referee's comment, the response on the referee's previous comment about "How the friction velocity (or wall shear stress) is calculated"? And "How accurate is the calculated value?" is added to the manuscript text and highlighted with the yellow color. In addition, Figure 1 of the response is placed in the manuscript as Figure 3. The new sentences are added to the manuscript as below:

"y^+ is the non-dimensional wall distance for a turbulent boundary layer defined as $y^+ = \frac{\rho u_f y}{\mu}$ (Shojaeefard et al. 2012) and friction velocity u_f is calculated as $u_f = \sqrt{\tau_w / \rho}$. In this equation, ρ is the density and τ_w is the wall shear stress. To find the accuracy of the calculated value for the wall shear stress, the skin friction coefficients C_f of upper and lower surfaces of the NACA0012 airfoil computed with the two-dimensional K-ω SST, are compared to the Iovnovich & Raveh's (2012) RANS simulation results. In both studies, simulations are performed based on McDevitt & Okuno's (1985) wind-tunnel test case with the Mach number of 0.75 and angle of attack of 2° (see Table 1, Set 1). As it is seen in Figure 3, there is a good validity between the computed and Iovnovich & Raveh's (2012) results.

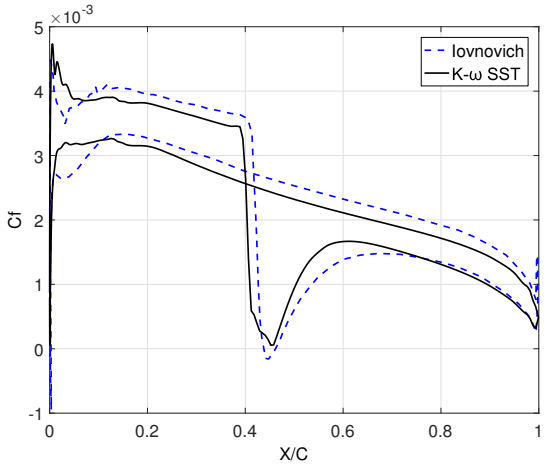

Figure 1 Skin friction coefficient variation of the NACA0012 airfoil, comparison of the K-ω SST and Iovnovich & Raveh's (2012) results.

"